

Utilizing Full UHPC Compressive Strength in Steel Reinforced UHPC Beams

Y. Shao & S. L. Billington

Department of Civil and Environmental Engineering, Stanford University, Stanford, CA, USA

Abstract: Steel reinforced ultra-high performance concrete (R/UHPC) flexural members commonly fail by fracture of the steel reinforcement after crack localization rather than crushing of the cement-based matrix as expected in traditional reinforced concrete. When failing after crack localization, R/UHPC specimens show low drift capacity and the high composite compressive strength is not utilized. In an effort to develop design approaches that might fully utilize the high compressive strength of UHPC and guarantee a minimum drift capacity, this study investigates an R/UHPC flexural element failing by crushing. Four-point bending tests are performed on two R/UHPC beams that are designed to fail in one case after crack localization and in the other after UHPC crushing. Experimental measurements include load, mid-span deflection, UHPC surface strain, and reinforcement strain. Surface strains are used to characterize compressive zone behavior for an ultimate strength prediction. Test results demonstrate that the R/UHPC specimen that failed after crushing had a larger drift capacity than the R/UHPC specimen that failed by fracture of the reinforcement after crack localization. The maximum compressive strain in the UHPC at crushing was measured to be 0.0065, at which point the reinforcement had significantly strain hardened. The observed compressive zone behavior and reinforcement behavior are incorporated into a new proposed strength prediction method.

Keywords: UHPC, Crushing, Maximum Compressive Strain, Flexure, Drift, Crack Localization, Strength Prediction

1. Introduction

Designed using packing density theory (Richard and Cheyrezy 1995), ultra-high performance concrete (UHPC) is a class of material that usually shows a compressive strength larger than 22 ksi (150 MPa). To mitigate the intrinsic brittleness of UHPC, short and randomly distributed fibers are added to the UHPC material (see review in Yoo and Banthia 2016). When designed for structural members, steel reinforcing bars and/or fiber-reinforced polymeric (FRP) reinforcing bars are also incorporated to improve the composite behavior (e.g., Yoo and Yoon 2016). Due to its higher compressive strength and bond strength than conventional concrete, UHPC has been proposed for use in bridge girders (e.g., Graybeal 2008, Steinberg 2009), bridge decks (e.g., Hwang et al., 2009, Shao et al., 2017), and cast in-situ connections (e.g., Graybeal 2015, Tazarv and Saïdi 2015).

R/UHPC flexural members are most often reported to have failed after the formation of one or two localized cracks (Meade and Graybeal 2010, Yang et al., 2010, Yoo et al., 2017, Chen et al., 2017, Hasgul et al., 2018, Stürwald 2018). After the initiation of this crack localization, the loss of fiber-bridging capacity leads to a loss in load-carrying capacity (Figure 1), which may result in drift capacities as low as 1.8% (e.g., Meade and Graybeal 2010, Yang et al., 2010, Yoo et al., 2017). When R/UHPC beams fail after crack localization, the peak load is essentially the load reached when the crack begins to localize. At this point the maximum compressive strain may be

as low as 0.001 and 0.0016 (e.g., Yoo et al., 2017). The low compressive strain and beam failure implies that oftentimes less than one-third of the compressive strength is utilized at the peak load.

For other types of high-performance fiber-reinforced-concrete, often referred to as HPFRC and exhibiting compressive strengths significantly lower than UHPC, two different failure paths have been reported (Figure 1): failure after crack localization as reviewed above (see for example, Tavallali et al., 2014, Bandelt and Billington 2016) or failure after crushing (e.g., Fischer and Li 2002, Bandelt and Billington 2016). To date few studies have reported the response of R/UHPC flexural members failing by crushing of the UHPC (Stürwald 2018). In order to utilize the high compressive strength of UHPC, it is desired to explore the crushing failure of R/UHPC.

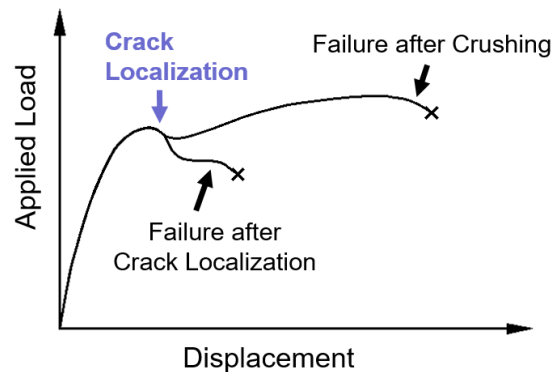


Figure 1. Schematic of the Two Failure Paths

This study compares two simply-supported R/UHPC flexural elements incorporating steel fibers and failing in different modes. The first, with a reinforcing ratio of 2.1% is designed to fail by crushing of the R/UHPC and the second with a reinforcing ratio of 0.96% is designed to fail by reinforcement fracture after crack localization. Experimental measurements include load, mid-span deflection reported in terms of drift, reinforcement strain, maximum crack width, surface strain, and curvature. The experimental results are compared with a proposed strength prediction method.

2. Experimental Program

2.1. Materials

Table 1 lists the mix proportions of the UHPC material investigated. The mixture contained steel fibers with a length of 0.51 in. (13 mm) and a diameter of 0.0079 in. (0.2 mm), which represented 2% of the mixture volume. Each reinforced beam was cast with a separate batch due to the limited capacity of the mixer. The material was mixed in a horizontal shear mixer, and placed into one end of a beam mold and allowed to flow to the other end. The beams were moisture cured for 8 weeks to reduce shrinkage strains after which they were air cured. The beams were tested at 24 weeks at which time no shrinkage cracking was observed on the beam surface.

Table 1. Mix Proportion

	lb/yd ³	kg/m ³
Pre-blended mix	3700	2195
Admixture	50.6	30
Steel fiber	262.9	156
Water	193.8	115

As per ASTM C1856-17, two unreinforced beams and three cylinders were cast and tested along with each reinforced beam to obtain the flexural strength and compressive strength of the UHPC. The unreinforced beams had a section of 3 in. by 3 in. (76 mm by 76 mm) and a span of 9 in. (228 mm) and were subjected to third-point bending. Figure 2(a) shows the load-displacement response of the two unreinforced beams for each beam cast. Batch 1 was used to cast beam UHPC-0.96 and Batch 2 was used to cast beam UHPC-2.10. The cylinders had a diameter of 3 in. (76 mm) and a height of 6 in. (152 mm), and were subjected to uniaxial compression. The average compressive strength of the two batches was 18.6 ksi (127.9 MPa) with a standard deviation of 0.6 ksi (4.5 MPa).

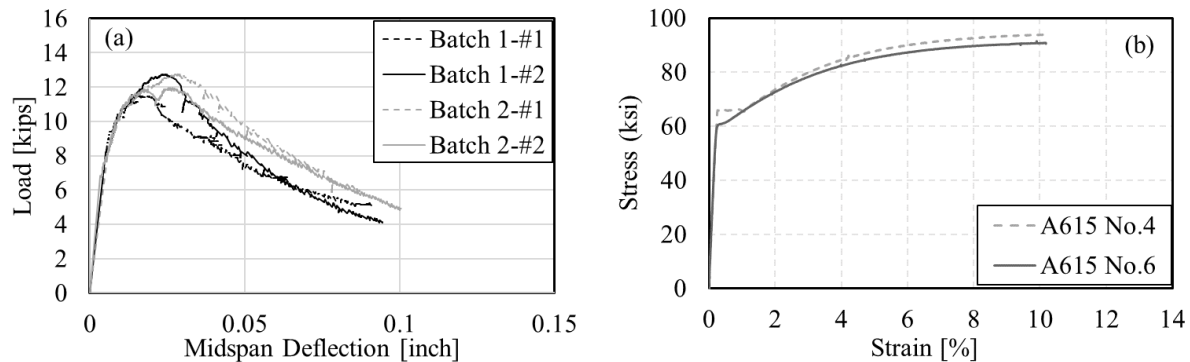


Figure 2. Material Behavior: (a) Load-deflection Response of the Unreinforced UHPC Beams; (b) Tensile Stress-strain Response for the Longitudinal Reinforcing Steel. (1kip=4.44 kN, 1 inch =25.4 mm)

The longitudinal reinforcement was A615 Grade 60 steel. Three steel coupons were tested in a 220-kip (978 kN) MTS machine to obtain the tensile response of each of the two bar sizes used in the beams. Figure 2(b) shows a representative stress-strain response for each bar size. An extensometer with a gauge length of 2 in. (50 mm) measured the steel strain. The extensometer was removed before steel fracture. As per the manufacturer, the steel fracture strain was expected to be 15-16%. Shear stirrups were Grade 60 steel with a diameter of 0.37 in. (9.5 mm).

2.2. Specimen Design and Test Setup

The specimen design and test setup are shown in Figure 3. The naming convention for the beams is based on the reinforcing ratio: UHPC-0.96 had a reinforcing ratio of 0.96% provided by two No. 4 bars with a diameter of 0.50 in. (12.7 mm) while UHPC-2.10 had a reinforcing ratio of 2.10% provided by two No. 6 bars with a diameter of 0.75 in. (19.1 mm). The shear stirrups had a spacing of 3.5 in. (90 mm) in the middle span with a reduced spacing of 1.8 in. (45 mm) near the supports.

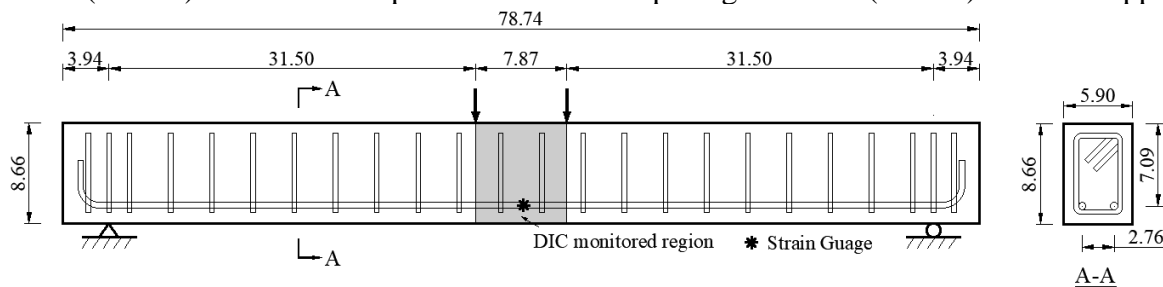


Figure 3. Specimen Design and Test Setup. (Unit: inch; 1 inch=25.4 mm)

The beams were tested under monotonic loading at a rate of 0.0038 in./s (0.097 mm/s). The constant moment region was monitored on one side by a digital image correlation (DIC) system to measure the surface strain, maximum crack width, and curvature. The surface strain and curvature were measured by creating extensometers in the DIC system over the constant moment region (i.e., the length of the extensometers was 7.87 in. (200 mm)). The maximum crack width was measured by creating an extensometer that bridged the localized crack in the DIC system. Mid-span displacement was measured by the average of readings from two string pots. One strain gauge was attached to the middle of each longitudinal bar (i.e., two strain gauges for each beam), and the averaged readings are reported.

3. Results and Discussion

3.1 Load vs. Drift Response and Crack Patterns

The load-drift response and the maximum crack width history of beams are shown in Figure 4, where drift is defined as the ratio of the mid-span deflection (Δ) to the shear-span length ($L_{\text{shear-span}}$). The crack patterns just prior to failure in each beam are shown in Figure 5. For beam UHPC-0.96, the load-drift response was linear until reaching a load of 12.1 kips (53.7 kN), at which point a cracking noise was heard but no visible cracks were found. Visible hairline cracks appeared when the load reached 18.0 kips (80.0 kN). The longitudinal steel yielded at a load of 23.9 kips (106.1 kN). Shortly after steel yielding, one of the multiple fine cracks (Figure 5) localized and the beam reached its peak load of 28.9 kips (128.3 kN). At the peak load, the maximum crack width was 0.0078 in. (0.2 mm). This crack width was also observed to be the maximum crack width that led to crack localization and loss of fiber-bridging capacity in the unreinforced beam tests (Figure 2(a)). After reaching the peak load, the localized crack continued to open and the load gradually decreased until the longitudinal reinforcement fractured (denoted by the 'x' in Figure 4). This failure path is referred to as 'failure after crack localization' (Figure 1) and as stated earlier has been observed in previous research on R/UHPC beams in flexure.

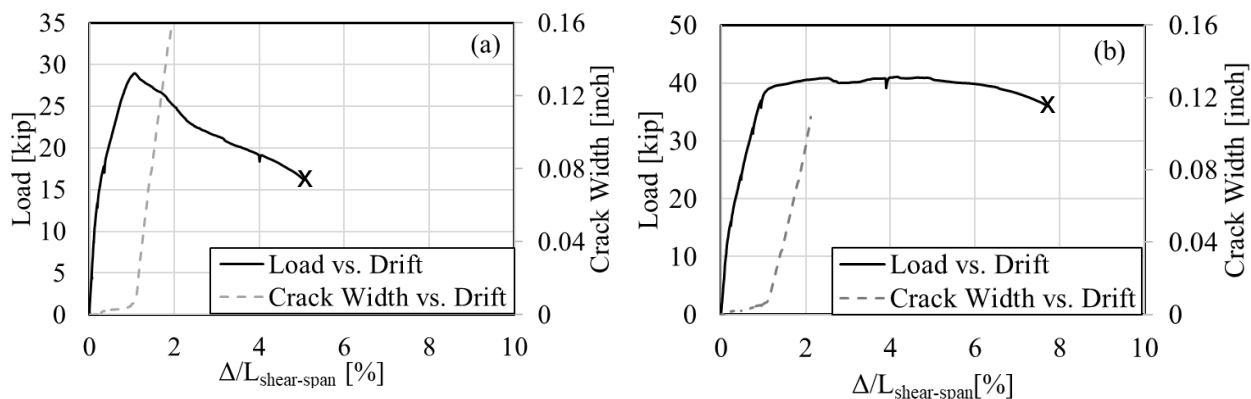


Figure 4. Load-drift Response and Maximum Crack Width History for: (a) Beam UHPC-0.96, and (b) Beam UHPC-2.10. (1kip=4.44 kN; 1 inch=25.4 mm; 'X' represents reinforcement fracture)

Increasing the reinforcing ratio from 0.96% to 2.10% changed the failure path of R/UHPC from one of failure after crack localization to failure after crushing (Figure 1 and 4). For beam UHPC-2.10, the load-drift response was linear up to a load of 12.7 kips (56.4 kN). Similar to beam UHPC-0.96, a cracking noise was heard but no visible cracks were observed until the load reached 17.3 kips (77.0 kN). The steel yielded at a load of 31.3 kips (139.0 kN) followed by a single

dominant crack forming at a load of 39.0 kips (173.2 kN) (Figure 5). Fiber-bridging was then gradually lost with increasing load. Unlike the case of UHPC-0.96, the loss of fiber-bridging capacity did not lead to a decrease in load capacity for UHPC-2.10. Instead, the longitudinal reinforcement strain hardened, and the load gradually increased until the UHPC began to crush at a load of 41.1 kips (182.7 kN), which corresponded to a drift of 4.2%. The longitudinal steel strain gauges stopped recording after the drift reached 2.4% with a corresponding average strain of 1.76%. After crushing of the UHPC, the load gradually decreased and finally the reinforcing bar fractured. This failure path is termed as ‘failure after crushing’ (Figure 1) and demonstrates a design where the full compressive strength of the UHPC is utilized by the beam.

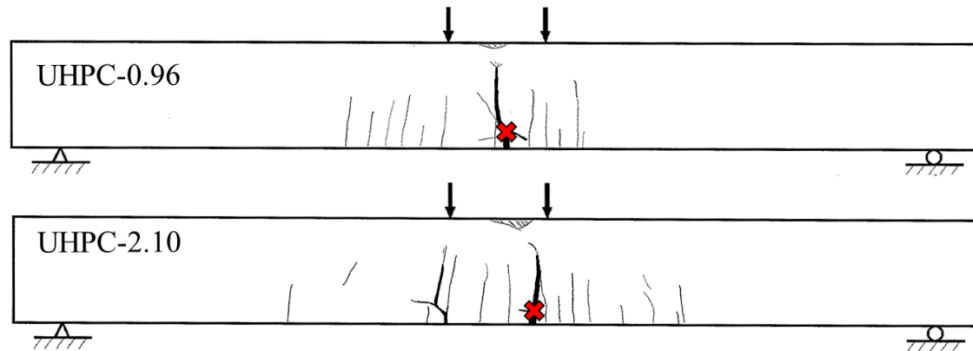


Figure 5. Crack Pattern before Reinforcement Fracture ('X').

3.2 Compressive Strains at Failure

Figure 6 shows the constant moment region of the two beams at their peak load. Beam UHPC-0.96, which failed after crack localization, exhibited no compressive damage at peak load, the crack widths were small (i.e., 0.0077 in. or 0.2 mm), and the drift was 1.1%. At the peak load of UHPC-2.10, which failed after gradual strain hardening of steel reinforcement, crushing occurred, the localized crack with a width larger than 0.0077 in. (0.2 mm) extended to about 75% of the specimen height, and the drift was 4.2%. Increasing the reinforcing ratio from 0.96% to 2.10% changed the failure path from failure after crack localization to failure after crushing, and provided more warning (i.e., compressive damage, cracking, and deflection) before failure.

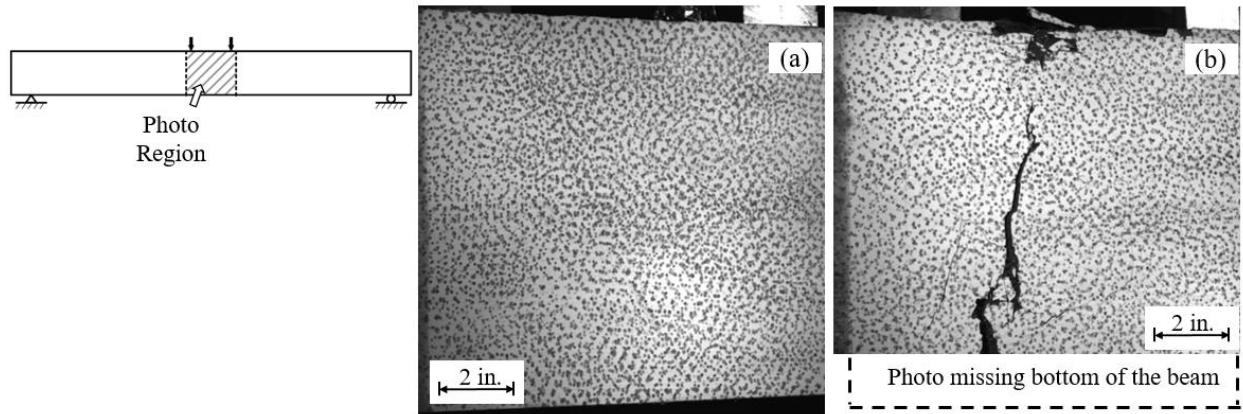


Figure 6. Cracking Behavior of Constant Moment Region at Peak Load for beams (a) UHPC-0.96, and (b) UHPC-2.10. (1 inch=25.4 mm)

Figure 7 shows the measured surface strain along the height at the peak load for each of the beams. For UHPC-2.10, the maximum compressive strain measured was -0.0065 , which is larger than the peak strain values reported from cylinder tests, which fall between -0.0027 and -0.0052 for UHPC-class materials (Haber, et al., 2018). For UHPC-0.96, the maximum compressive strain measured was -0.0014 . While these are results from just two beams, they indicate as might be expected that the peak cylinder-based compressive strain is not reached when beams fail by crack localization and is exceeded when flexural failure by crushing is reached as might be expected in a plastic hinging region of a flexural element.

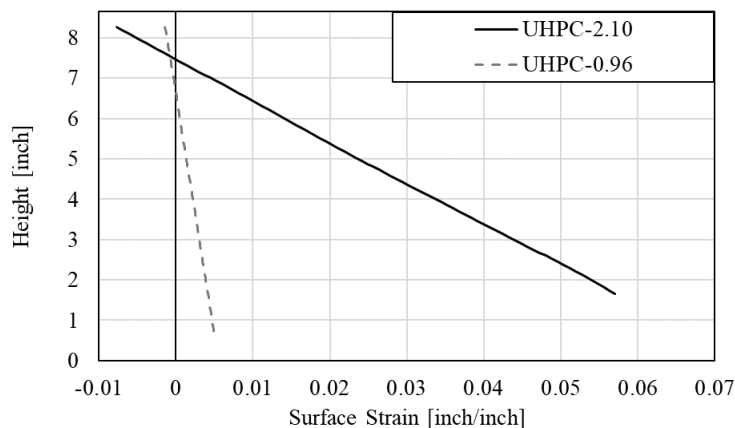


Figure 7. Measured Surface Strain Along the Beam Height at Peak Load

3.3 Summary of the Two Different Failure Modes

The experimental results presented in sections 3.1 and 3.2 demonstrated that:

1. For failure after crack localization, the peak load is reached when strain localizes in a single dominant crack, at which point the steel has just yielded, the maximum compressive strain is small (less than 0.0016), and fiber-bridging occurs over the entire tension zone.
2. For failure after crushing, the peak load is reached when the matrix begins to crush (strains greater than 0.0065), at which point the steel has significantly strain hardened and the fiber-bridging across the dominant crack is lost in most of the tension zone.

4. Flexural Strength Prediction - Hand Method

The differences in failure modes observed in section 3 and summarized in section 3.3 indicate that traditional strength-based prediction methods for nominal moment capacity do not directly apply as the limit states (e.g., maximum compressive strain at peak load) are different with R/UHPC.

Figure 8 presents a proposal for different limit state strains to adopt to represent the distinct mechanisms of the two failure paths and provide a quick hand method for estimating the flexural strength of a R/UHPC member. For failure after crack localization, the nominal moment capacity may be assumed to occur when the strain at the tension reinforcing steel reaches the crack localization strain ϵ_{loc} of the UHPC. This approach differs from current methods where strength is calculated assuming the UHPC has reached an user- or method-specified extreme compression fiber strain ϵ_{cu} (e.g., JSCE 2008, AFNOR 2016, Hasgul et al., 2018). In the proposed model, the steel stress is assumed to be the yielding strength, and fiber-bridging is assumed to act over the entire tension zone.

For failure after crushing, the nominal moment capacity may be assumed to occur when the maximum compressive strain reaches the crushing strain of the UHPC, ϵ_{cu} . In addition, reinforcing steel strain-hardening should be accounted for in the analysis and fiber-bridging is neglected based on experimental results reported in section 3. This approach differs from current methods where strain hardening of steel is neglected and the fiber-bridging is assumed to exist in most of the tension zone (e.g., JSCE 2008, AFNOR 2016, Hasgul et al., 2018).

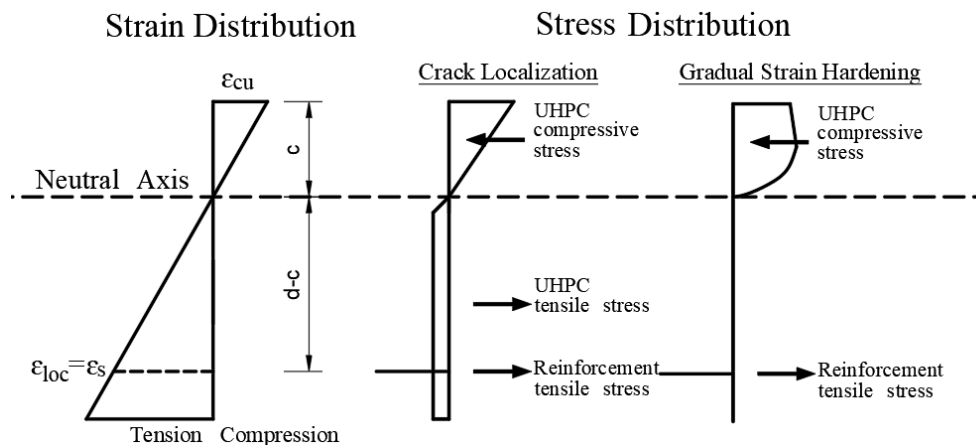


Figure 8. Strain and Stress Distributions for a Proposed Flexural Strength Prediction Method.

Applying the proposed strength prediction model to beam UHPC-0.96, the UHPC compressive model is assumed to be linear as UHPC compressive stress-strain response is typically linear up to 50% of the compressive strength (Haber et al., 2018), which corresponds to the compressive strains at peak load (0.001-0.0016) observed in beams failing after crack localization. The composite tensile behavior is assumed to be elastic-perfectly-plastic with effective tensile strength f_t being the localization stress, which is a common assumption (e.g., JSCE 2008, AFNOR 2016, Baby et al., 2017, Yoo et al., 2017). Here, the localization strain (ϵ_{loc}) and effective tensile strength (f_t) were assumed to be 0.002 and 11.5 MPa, respectively, based on an inverse analysis of unreinforced beam test results (Figure 2(a)). For the peak strength (which occurs at the point of crack localization), the model predicts nominal capacity of 35.7 kip-ft (48.3 kN-m), which is 6% smaller than the experimental moment capacity of 37.9 kip-ft (51.3 kN-m).

For the strength prediction of beam UHPC-2.10, the ascending branch of the compressive model is modelled using a parabolic function based on Hognestad (1951) and also used by JSCE (2008); the descending branch is linear with a 10% strength reduction. In the model, the compressive strain at peak is assumed as 0.0035 based on tests of similar material (Haber et al., 2018) and ε_{cu} is taken as 0.0065 based on the experimental findings reported in section 3. For the steel hardening model, the measured stress-strain curve presented in Figure 2(b) is used. For the peak strength prediction (which occurs at the point of UHPC crushing), the model predicts nominal capacity of 46.3 kip-ft (62.6 kN-m), which is 14% smaller than the experimental moment capacity of 53.9 kip-ft (73.0 kN-m). An improved knowledge of the compressive zone behavior, for example, the crushing strain and compressive stress distribution, will help improve the prediction accuracy.

5. Conclusions

A demonstration of changing the failure mode of R/UHPC flexural members from one of crack localization leading to steel fracture to one of UHPC crushing is presented by increasing the reinforcing ratio from 0.96% to 2.10%. For failure after crack localization, the initiation of crack localization (i.e., loss of fiber-bridging capacity) represents the peak load and capacity decreases thereafter followed by longitudinal steel fracture. At the peak load, the drift is small (1.1%), the steel has yielded, fiber-bridging is maintained within the tension zone, and maximum compressive strain is small (i.e., 0.0014). The high compressive strength is not fully utilized. For failure after crushing, the peak load occurs when the UHPC crushes followed by longitudinal steel fracture. At the peak load, the drift is large (4.2%), the longitudinal reinforcing steel has significantly strain hardened, fiber-bridging is lost in most of the tension zone, and the maximum compressive strain is large (0.0065). The maximum compressive strength of UHPC is reached and fully utilized for failure after crushing.

When reaching the maximum load capacity, failure after crushing provides more warning signs and represents different mechanisms than failure after crack localization. A strength prediction method that considers the observed failure mechanisms is presented and demonstrated to predict the experimental strengths within 6-14%. More experiments are needed to fully characterize the compressive zone behavior for R/UHPC flexural members that fail after crushing and improve the nominal capacity prediction method. More advanced methods, such as moment-curvature analysis and finite element analysis, are also expected to improve the prediction of failure mechanisms and prediction of flexural behavior.

6. References

- Building code requirements for reinforced concrete, ACI 318-14, American Concrete Institute (ACI), USA, 2014
- National addition to Eurocode 2 — Design of concrete structures: specific rules for Ultra-High Performance Fibre-Reinforced Concrete (UHPRC), NF P 18-710, Association Française de Normalisation (AFNOR — French standard institute), France, 2016.
- Standard Practice for Fabricating and Testing Specimens of Ultra-High Performance Concrete, ASTM C1856-17, ASTM int, US, 2017
- Baby, F., Marchand, P., and Toutlemonde, F., "Analytical Modeling of Ultra-High-Performance Fiber-Reinforced Concrete Behavior in Ribbed Plates." *ACI Struct. J.*, 114(1), 3, 2017.
- Bandelt, M. J., and Billington, S. L., "Impact of Reinforcement Ratio and Loading Type on the Deformation Capacity of High-Performance Fiber-Reinforced Cementitious Composites Reinforced with Mild Steel." *Journal of Structural Engineering*, 142(10), 14, 2016.

- Chen, S., Zhang, R., Jia, L.-J., and Wang, J.-Y., "Flexural behavior of rebar reinforced ultra-high performance concrete beams." *Magazine of Concrete Research*, 1-19, 2017.
- Fischer, G., and Li, V. C., "Effect of matrix ductility on deformation behavior of steel-reinforced ECC flexural members under reversed cyclic loading conditions." *Structural Journal*, 99(6), 781-790, 2002.
- Graybeal, B. A., "Flexural behavior of an ultrahigh-performance concrete I-girder." *Journal of Bridge Engineering*, 13(6), 602-610, 2008.
- Graybeal, B. A., "Splice length of prestressing strands in field-cast UHPC connections." *Mater. Struct.*, 48(6), 1831-1839, 2015.
- Haber, Z. B., De la Varga, I., Graybeal, B. A., Nakashoji, B., and El-Helou, R., "Properties and Behavior of UHPC-Class Materials." *FHWA-HRT-18-036*, 2018.
- Hasgul, U., Turker, K., Birol, T., and Yavas, A., "Flexural behavior of ultra-high-performance fiber reinforced concrete beams with low and high reinforcement ratios." *Structural Concrete*, 1-14, 2018.
- Hwang, H.-H., Yoo, D.-M., Park, S.-Y., and Kim, B.-S., "Optimized Design of UHPC Bridge Deck Slab for Hybrid Cable-Stayed Girder Bridge." *Proc., Proceeding of 13th REAAA Conference*, 04-19, 2009.
- Recommendations for Design and Construction of High Performance Fiber Reinforced Cement Composites with Multiple Fine Cracks (HPFRCC), Concrete Engineering Series 81, Japanese Society of Civil Engineering (JSCE), Japan, 2008.
- Meade, T., and Graybeal, B. "Flexural response of lightly reinforced ultra-high performance concrete beams." *Proc., Proceedings of the Third International fib Congress and Exhibition Incorporating the PCI Annual Convention and National Bridge Conference*, Washington, DC., 2010.
- Richard, P., and Cheyrezy, M., "Composition of reactive powder concretes." *Cement and concrete research*, 25(7), 1501-1511, 1995.
- Shao, Y., Shao, X., Li, L., and Wu, J., "Optimum Combination of Bridge and Deck Systems for Superspan Cable-Stayed Bridges." *Journal of Bridge Engineering*, 23(1), 04017112, 2017.
- Steinberg, E., "Structural reliability of prestressed UHPC flexure models for bridge girders." *Journal of Bridge Engineering*, 15(1), 65-72, 2009.
- Stürwald, S., "Bending Behaviour of UHPC Reinforced with Rebars and Steel Fibres." *High Tech Concrete: Where Technology and Engineering Meet*, Springer, 473-481, 2018.
- Tavallali, H., Lepage, A., Rautenberg, J., and Pujol, S., "Concrete beams reinforced with high-strength steel subjected to displacement reversals." *ACI Struct. J.*, 111(5), 1037-1048, 2014.
- Tazarv, M., and Saiidi, M. S., "UHPC-filled duct connections for accelerated bridge construction of RC columns in high seismic zones." *Engineering Structures*, 32-11, 3478-3487, 2010.
- Yang, I. H., Joh, C., Kim, B.-S., "Structural behavior of ultra high performance concrete beams subjected to bending" *Engineering Structures*, 73, 267-280, 2016.
- Yoo, D.-Y., and Banthia, N., "Mechanical properties of ultra-high-performance fiber-reinforced concrete: A review." *Cement and Concrete Composites*, 73, 267-280, 2016.
- Yoo, D.-Y., Banthia, N., and Yoon, Y.-S., "Experimental and numerical study on flexural behavior of ultra-high-performance fiber-reinforced concrete beams with low reinforcement ratios." *Can. J. Civ. Eng.*, 44(1), 18-28, 2017.
- Yoo, D.-Y., and Yoon, Y.-S., "A review on structural behavior, design, and application of ultra-high-performance fiber-reinforced concrete." *International Journal of Concrete Structures and Materials*, 10(2), 125-142, 2016.

7. Acknowledgements

The authors gratefully acknowledge the financial support of the Charles H. Leavell fellowship and the John A. Blume Earthquake Engineering Center at Stanford University. The authors also gratefully appreciate the material donations from and discussions with LafargeHolcim Ltd.